# Fluid-structure interaction analyses of a composite windsurf fin

L.S. Sutherland, M. Cardoso de Brito
*CENTEC, Instituto Superior Técnico, University of Lisbon, Portugal*

J. Chaves Pereira
*LAETA, IDMEC, Instituto Superior Técnico, University of Lisbon, Portugal*

M.R. Arruda
*CERIS, Instituto Superior Técnico, University of Lisbon, Portugal*

S. Benson
*MOST, Newcastle University, UK*

ABSTRACT: Numerical structural and fluid dynamic models of a windsurf fin were developed and validated using mechanical and water tunnel tests. Then, both a 'one-way' analysis (not including fin deformation fluid flow effects) and a full 'two-way' iterative fluid-structure interaction model (including fin deformation effects) combined the two. Finally, these models were used to investigate the fin behavior and performance for a range of typical sailing velocities and leeway-angles. The more expensive two-way model was required to accurately predict the lateral 'lift' and vertical forces, and tip twist, but the more economical one-way model gave good estimations of the drag force (especially at lower leeway angles) and tip deflection. Vertical fin forces became significant as the fin deflects. Both composite material bend-twist coupling giving wash-in (locally higher angles of attack) at higher lateral deflections, and flow modifications due to fin deformations that give wash-out (feathering) are thought to be active.

## 1 INTRODUCTION

Windsurfing equipment is capable of extremely high sailing speeds (over 50 knots (World Sailing Speed Record Council, 2021)) where little of the board is in contact with the water and in fact almost all of the hydrodynamic upwind side force required to counteract the aerodynamic downwind side force of the sail is supplied by the fin, or (lateral hydro-) 'foil' (Sutherland, 1993; Sutherland and Wilson, 1994). The only economically viable materials that can resist the resulting very high loadings are advanced fibre (mostly carbon with some E-glass) composites.

There are various basic fin designs for each intended sailing discipline - from control-biased wave sailing, through slalom, to speed-biased course racing. Control is usually achieved via 'twist-off' (wash-out) at the fin tip to progressively reduce angles of attack at high loadings, and is normally realised via aft-swept planforms and aft rake to give the typical 'dolphin fin' shape of the wave fin. The hydrodynamically more efficient upright course racing fins with elliptical planforms result in better lift to drag ratios at the expense of more sudden, and hence uncontrollable, stall behaviour. Slalom fins tend to aim at a compromise between these two extremes.

Hence, the fin is as important, if not more so, than the two other components of a windsurfer, the rig and the board. However, despite some scientific interest in the subject, mostly in the 1990's (Broers et al., 1992; Chiu et al., 1993, 1992; Fagg, 1997; Fagg and Velay, 1996a, 1996b; Kunoth et al., 2007), the development of modern fins has been almost entirely empirical via 'on-the-water' testing of new ideas. This approach is perhaps not surprising given the complexity of the problem in terms of fluid flow, complex anisotropic composite structural deformations, and the hydro-elastic interaction between the two.

Whilst this approach has greatly improved fin performance, further advances in fin design are hampered since exactly how this performance is achieved in terms of the deflections of the fin remains unseen under the board. There are theories within the windsurfing community, using vague 'semi-scientific' terms (for example, 'softness') and based on *perceived* physics of the problem, but the bases of these are often not very solid.

Hence, the current work develops a design tool using fluid structure interaction (FSI) hydro-elastic numerical analyses, as detailed in Section 2, to predict the actual fin responses of the fin to the hydrodynamic loadings under the board. The response of the fin to a range of typical sailing conditions is then explored using this FSI model and discussed in Sections 3 and 4.

## 2 NUMERICAL MODEL

### 2.1 *Fin characteristics*

This study models an actual production fin; a 37 cm slalom fin manufactured by F-Hot fins Ltd (Figure 1).


*Figure 1 Slalom fin geometry*

The port and starboard sides of the fin laminate are hand laid up separately using epoxy resin in the two parts of a split female aluminium mould that are then bought together, before the resin cures, and bolted together. The fin is then left to cure as a single piece at 50°C for 24 hours. The exact layup schedule is commercially sensitive information, but each side consists of 19 plies of ±45° bi-directional and 0° uni-directional (UD) carbon and E-glass tapes.

### 2.2 *Finite Element Analysis (FEA)*

ABAQUS finite element analysis software (ABAQUS, 2018) was used to model the structural response of the fin, mainly because of the ease with which it can be integrated into an FSI analysis (Section 2.5) with the CFD software used (section 2.4). Thickness measurements of an actual fin confirmed the accuracy of the input geometry, which was partitioned into segments corresponding to areas with the same layup (Figure 2).

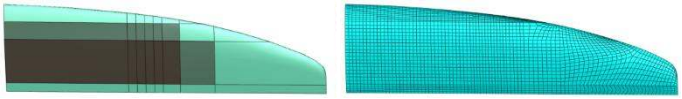

*Figure 2 FEA Partitions (shaded areas = UD tapes) and mesh*

SC8R general-purpose, 8-node, hexahedral, first-order, reduced-integration, continuum shell elements were used to both model precisely the complex fin geometry and to reduce computational expenses. This element accounts for finite membrane strains, arbitrary large rotation, and allows for changes in thickness, making it suitable for this large-strain / displacement analysis. The composite layup of each partition of Figure 2 was defined as an ABAQUS 'composite set', where the layup angles and thicknesses of each individual ply as in the actual fin were defined, allowing the laminate mesh to subdivide through the laminate thickness.

The SC8R element required hexahedral meshing, and since it is a first-order reduced-integration element, the mesh had to be sufficiently fine to avoid 'hour-glassing'. A nominal global mesh size of 4 mm, selected via a mesh sensitivity study, resulted in 13824 elements. The mesh was refined at the leading and trailing edges due to the increased curvature in these areas (Figure 2).

The fin is mounted in the board with a very stiff cantilever arrangement and so the FEA modelled fin foil section was restricted here with boundary conditions preventing both translation and rotations in all directions.

As further detailed below, for validation of the structural model single point loads were applied to one side of the fin only. For the FSI analyses of section 2.5 the pressure loadings on both faces obtained from the CFD model of section 2.4 were applied.

### 2.3 *Material properties and experimental FEA validation*

As is typical for marine composites, the fin laminates produced here are not the well-documented and regulated factory-impregnated 'pre-pregs' characteristic of the aerospace industry, and so material properties may not be simply obtained from laminate data sheets, and there are no (expensive) material properties testing programmes. Further, the fins are hand laid up. Hence, not only are there no available material properties data, but also their estimation is hampered by a lack of information on the ratio of fibres to resin, the fibre volume fraction (FVF). Hence, as is typical for marine composites, an 'engineering' approach had to be developed to estimate the material properties.

Firstly, measurements of the weights of fibres and resin used in the manufacture of a fin were taken, giving an FVF estimate of 0.4 from the known densities of the materials used, which corresponded with the lower ranges of FVF for hand laid up marine composites to be found in the literature (Sleight, 1985; Smith, 1990).

The material properties to be used should correspond to both the closest raw materials *and* fabrication methods used for the laminates studied. In this case, 'wet layup' (from the FVF's this was deduced to be vacuum assisted wet layup, which is similar to the compression moulded wet layup used here) values were obtained from the material property library of another FEA software, ANSYS (*ANSYS© 2020 R1*, 2020). A further advantage of these ANSYS library values is that they are experimentally based, and hence incorporate effects of the lay-up process that theoretical estimates will miss. It is unimportant from where these values originate, what *is* very important is that they are for *relevant* laminates. Young's Modulus, E, Poisson's Ratio, ν, and Shear modulus, G; each in all three orthotropic directions) for equivalent woven and UD carbon and UD E-glass were obtained.

However, these ANSYS library values corresponded to laminates of higher FVF (from 0.5 to 0.65)

than of those considered here (0.4) and so these library properties had to be adjusted for the difference in FVF. This was achieved using the generalised rule of mixtures (ROM) equations (Shenoi et al., 1993), which is known to be acceptably accurate for stiffness estimation. For example, for longitudinal stiffness, $E_1$, for two laminates 'A' & 'B' equivalent in all respects except for FVF (Vf):

$$E_{1,c} = \eta_0 \eta_L E_{1,f} V_f + E_m(1 - V_f) \quad (1)$$

and hence,

$$E_{1,c,B} = \frac{\eta_0 \eta_L E_{1,f} V_{f,B} + E_m(1 - V_{f,B})}{\eta_0 \eta_L E_{1,f} V_{f,A} + E_m(1 - V_{f,A})} \times E_{1,c,A} \quad (2)$$

where subscripts c, f and m refer to composite, fibre and matrix resin, respectively, $\eta_0 = 1.0$ for UD and 0.5 for woven reinforcements, and $\eta_L = 1.0$ (since fibre lengths > 10 mm).

This semi-empirical approach, rather than ROM estimation of the material properties directly from the fibre and resin properties, is based on experimentally obtained values thus factoring in irregularities introduced via hand lay-up, which are not considered by ROM.

The material property values thus obtained were then verified using values estimated using the Chamis semi-empirical equations (Chamis, 1984, 1983; Vignoli et al., 2019) directly from the resin and fibre material properties and a typical hand lay-up void fraction of 0.05 (Abdelal and Donaldson, 2018; Roopa et al., 2015). This gave values very close to the previously calculated 'ROM adjusted FVF' data in all cases, thus increasing confidence in the material property input data.

The next step was to validate the FEA model against experimental force-deflection data. A simple cantilever loading of the fabricated fin, as in the sailing condition was used, but reproducing the in-service force loading on the fin was not practical and hence a simplified point load was used. This load was applied at ¼ chord from the leading edge, coinciding with the centre of effort of the fin under flow conditions. Two separate tests were performed; at positions of 40 and 80 % of the span from the fin base (Nascimento et al., 2018) (Figure 3), giving differing proportions of shear and bending to provide a more rigorous validation of the FEA model than is often given. A calibrated, displacement controlled (at 0.1 mm/s), servo-hydraulic test rig with load cell and displacement transducer outputs was used.

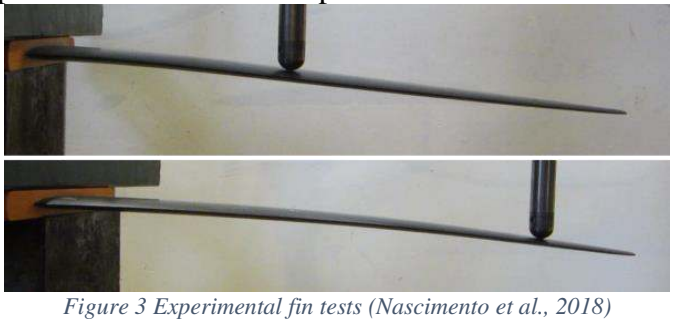

*Figure 3 Experimental fin tests (Nascimento et al., 2018)*

However, these tests showed that the FEA model was predicting a less stiff response than shown to be the case by the experimental results. Hence, further discussions with the manufacturer and observations of the lamination process were undertaken, after which it was noted that the plies were not actually laid up in the mould with the fibres exactly straight and aligned with the fin span, but were curved to some degree. This occurred due both to natural fibre movements during the rolling stage of hand layup, and to the process of fitting the plies into the mould with its curved leading edge plan shape.

Even a slight curvature of the plies in the laminate is known to decreases the stiffness in the fibre direction, and typical fibre 'waviness' was measured as approximately 2.5 mm amplitude in a wavelength of 10 cm, giving a Young's modulus reduction factor of 0.25 according to Figure 3.1 of (Altmann, 2015). This reduction was applied to all UD and woven longitudinal and woven transverse Young's modulus, E, values, to give final material properties shown in Table 1.

This gave extremely good agreement with the experimental values for both point-loading spans (Figure 4). Thus the FEA model has been validated for both different loading cases and the input material values were obtained considering both the actual raw materials *and* the production process and resulting laminate characteristics, rather than simply carrying out a 'curve fitting' exercise to force the model to fit the experimental data, which has unfortunately become commonplace.

| Property | UD E-glass | UD Carbon | Woven Carbon |
|---|---|---|---|
| $E_1$ (Pa) | 2.23E10 | 5.66E10 | 2.84E10 |
| $E_2$ (Pa) | 7.90E9 | 5.11E9 | 2.84E10 |
| $E_3$ (Pa) | 7.90E9 | 5.11E9 | 5.54E9 |
| $v_{12}$ | 0.29 | 0.31 | 0.04 |
| $v_{23}$ | 0.40 | 0.42 | 0.30 |
| $v_{13}$ | 0.29 | 0.31 | 0.30 |
| $G_{12}$ (Pa) | 4.12E9 | 3.26E9 | 3.30E9 |
| $G_{23}$ (Pa) | 3.50E9 | 3.08E9 | 2.70E9 |
| $G_{13}$ (Pa) | 4.12E9 | 3.26E9 | 2.70E9 |

*Table 1 Material Property values*

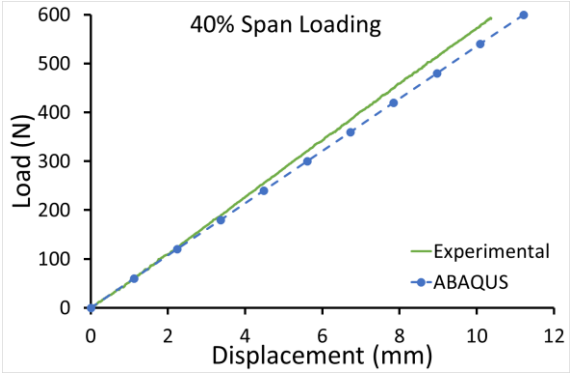

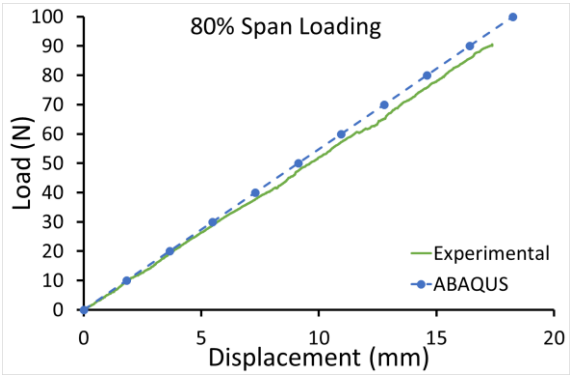


*Figure 4 Validation of FEA with experimental test results*

## 2.4 *Computational Fluid Dynamics (CFD) Analysis*

Star-CCM+ software (*Siemens Simcenter STAR-CCM+ Documentation*, 2019) was used which integrates seamlessly with ABAQUS FEA software for FSI analyses. The analysis here is developed from the results of a previous study (Saldanha, 2019). Although to eliminate numerical singularities the sharp leading edge of the FEA geometric model had to be slightly rounded for the CFD, this extremely localised and small geometry change would not cause discrepancies between FEA and CFD results.

The fluid domain was a rectangular prism of dimensions 16 x 10 x 8 fin base chord lengths, with the fin base located on the upper face, centred laterally and 6 base chord lengths from the inlet face (Figure 5).

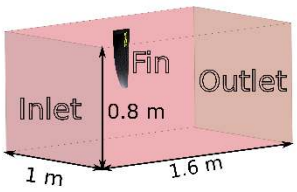


*Figure 5 CFD Fluid domain*

The boundary conditions were 'Wall' for the fin surface, 'Pressure Outlet' for the outlet aft face, and 'Velocity Inlet' for the inlet, lateral faces and bottom face, where there are unperturbed flow conditions. Although the fin base is actually inserted into the flat underside of the board, since the boundary layer at the board is less than 1 cm thick the finite extent of the board was not modelled and the whole upper domain face was assigned as a 'Velocity Slip Wall' with zero vertical velocities representing the water-air interface. This significantly reduced computational time and complexity and confirmatory tests showed that this did not affect the results. The 'Velocity Inlet' flows were assigned to give the angle of attack to the fin required.

To model accurately the flow whilst also saving computational expense, the 'Automated Mesh' feature of Star-CCM+ was used to mesh the domain, with increasingly finer volumes of refinement (VOR's) from the outer domain down to the fin surface (Figure 6). Since the analysis of the flow of the boundary layer is especially important, a prism layer that closely followed the fin profile was used next to the fin surface. Table 2 gives the mesh parameters, which were previously validated by a mesh convergence analysis (Saldanha, 2019).

The physical continuum models used were: (Saldanha, 2019):

- Three-dimensional analysis
- Steady and segregated flow
- Constant density
- Turbulent flow solution with RANS (Reynolds-Average Navier-Stokes) equations
- K-ω, SST (Menter) turbulence model
- γ−Reθ transition model
- Low y+ wall treatment

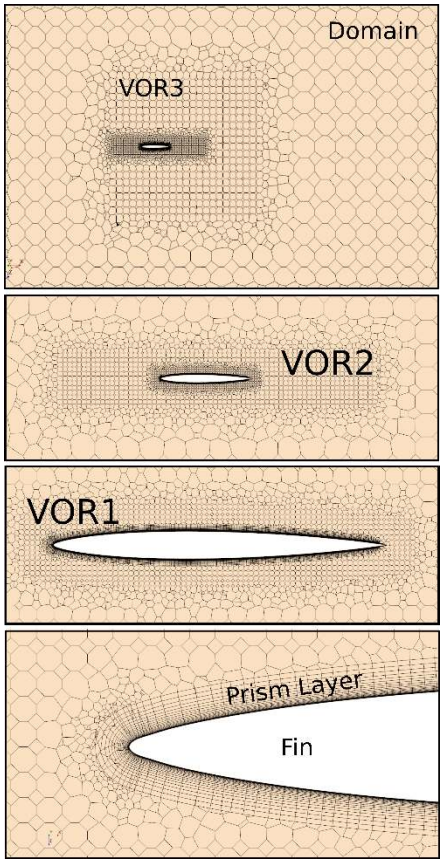


*Figure 6 CFD Mesh*

| | |
|---|---|
| Base size | 50 mm |
| Domain Relative Cell Size | 150% |
| VOR 3 Relative Cell Size | 50% |
| VOR 2 Relative Cell Size | 10% |
| VOR 1 Relative Cell Size | 3% |
| Number of Prism Layers | 25 |
| Prism Layer Thickness | 2 mm |
| Prism Layer Stretching | 1.17 |
| Wall y+ | ≈1 |
| Number of Cells | ≈ $3x10^6$ |

*Table 2 Mesh Parameters*

The fluid assumed for all simulations was 35 g/kg salinity seawater at 20 °C, of density ($\rho$) 1024.9 kg/$m^3$

and dynamic viscosity ($\mu$) 1.077x10$^{-3}$ Pa · s (Nayar et al., 2016). Residuals convergence criteria (at 10$^{-4}$) gave solutions that required around 180 computational hours running in 18 parallel cores, i.e. an elapsed real time of 10 hours.

### 2.5 *Fluid structure interaction (FSI) analysis*

The hydrodynamically efficient fine chord profiles of these fins together with the high loadings lead to large deflections, and hence a simple 'one-way' analysis (where CFD derived loads assuming a completely rigid fin are applied in a single step solution to the structural model to give the structural response) may well lead to large errors. A full 'two-way' FSI analysis where iterative re-application of the CFD loads to the structural model until convergence is achieved will more closely model such a hydro-elastic case.

The FEA and CFD models of sections 2.2 and 2.4 were connected via the Simulia Co-Simulation Engine (CSE), which enables fully automatic communication between the two for import and export of field properties and mesh information. The CSE required that the same fin surface was present and with the same name in both CFD and FEA solvers. In this region, displacements are exported from FEA to CFD solvers, and pressures and wall shear stresses exported in the opposite direction (ABAQUS, 2018). It is important to use the same units in both solvers.

Since significant fin deflections were expected, an iterative dynamic implicit approach was used where fields are exchanged multiple times per coupling step until an overall equilibrium is achieved prior to advancing to the next step. This iterative coupling scheme allows one analysis to lead, which, as highly recommended (*Siemens Simcenter STAR-CCM+ Documentation*, 2019), was the structural (ABAQUS) solver. A constant coupling step size of 0.1 s between FEA and CFD solvers, allowing both analyses to advance in parallel, achieved good solution convergence. Especially for operating conditions with higher fin deflections and pressures, and at the start of each simulation, ramping of the pressure field was also required to achieve solution convergence. As for the CFD analysis, residual convergence criteria at 10$^{-4}$ were used for the FSI analyses.

## 3 RESULTS

The behavior of the fin under a range of typical sailing conditions was explored using the FSI analysis tool. Two main parameters, velocity and lateral angle of attack (AoA, corresponding to 'leeway angle'), may be used to represent these conditions. A parametric study of all permutations of a range of pertinent velocities and AoA's was completed. The CFD analysis indicated that stall occurred at around 8° AoA, and a typical upper velocity is around 35 knots was assumed. Hence, the test matrix consisted of five levels of velocity (10, 15, 20, 25, 30 and 35 kn) at three levels of AoA (2, 4 and 6°).

To quantify the fin behavior the responses 'lift' (in the lateral, opposing sail side force sense) and drag forces give a good indication of the fin performance. Similarly, twist (thus varying the local tip AoA) and tip (cantilever) deflection, are important in terms of control.

Vertical force is important in terms of both first starting to plane and then supporting the weight of the board, rig and sailor. If the fin can produce some of this vertical force then this reduces the required AoA and/or wetted surface area of the board, resulting in less drag since the fin produces vertical force much more efficiently than can the inclined flat plate, hydroplane, board.

Especially as the fin is increasingly 'loaded up' at higher velocities and/or AoA's and deflections increase), a two-way FSI may well produce more accurate results than a one-way FSI. However, this will come at considerably increased time, software and expertise costs that will be very significant in the context of the windsurfing industry. Hence, it is important to identify where the use of a two-way FSI over a one-way analysis is, and is not, beneficial.

The results of runs at every combination of velocity and AoA for both 1-way and 2-way solutions for 'lift' and drag force, tip deflection and twist, and vertical force are given below in Figure 7, Figure 8, Figure 9, Figure 10 and Figure 11, respectively.

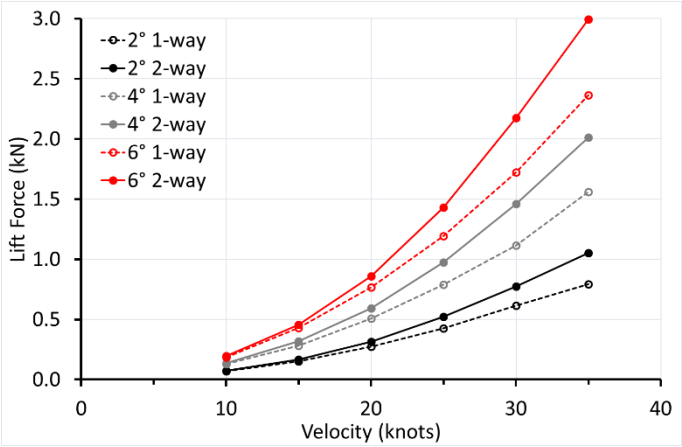


*Figure 7 'Lift' force results*

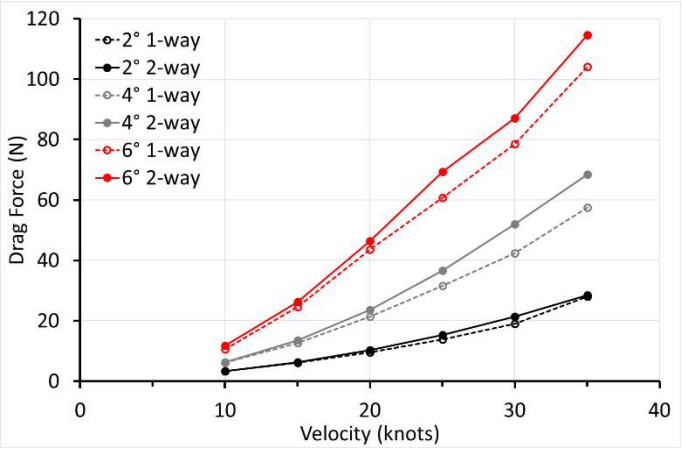


*Figure 8 Drag force results*

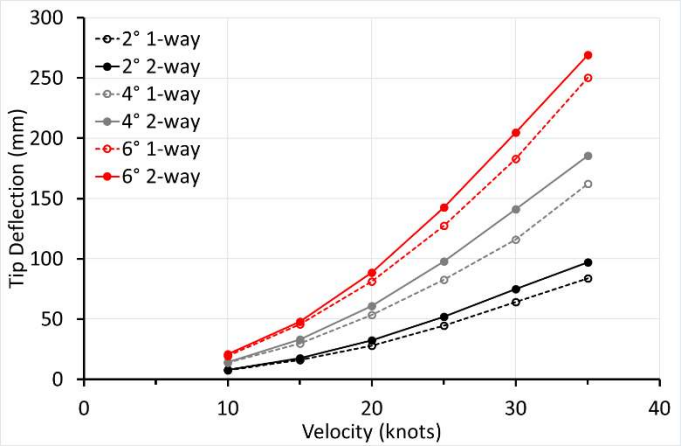


*Figure 9 Tip deflection results*

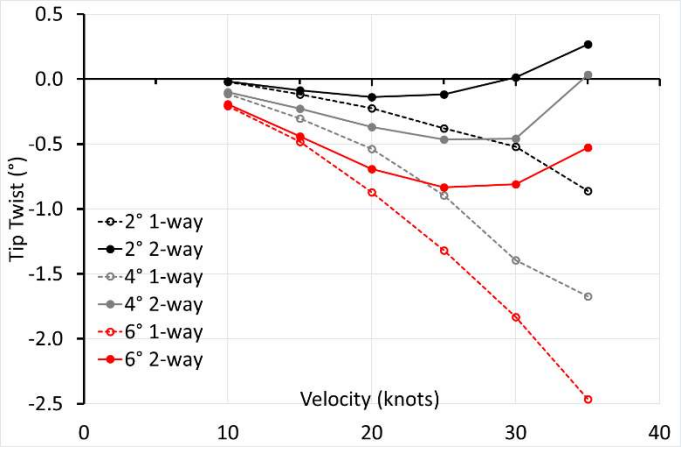


*Figure 10 Tip twist results (negative = wash-in = increased AoA)*

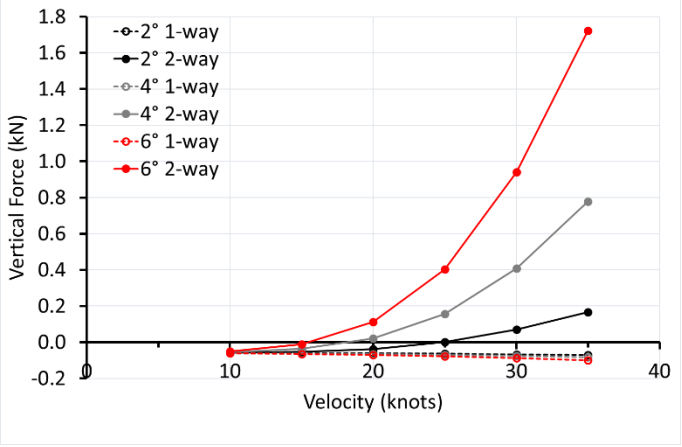


*Figure 11 Vertical upwards force results*

## 4 DISCUSSION

To validate the FSI model the fin was tested in the Emerson cavitation tunnel at Newcastle University, UK (Tansley, 2018). Figure 12 shows that the fin deflected significantly, even at the relatively low sailing speed of approximately 10 knots.

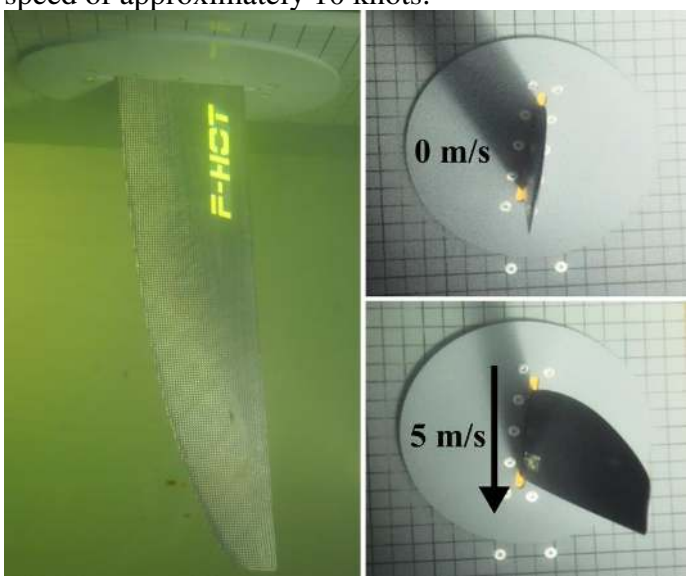


*Figure 12 Water tunnel test set-up*

Although the tests had to rely on manual logging of the lift force from analogue measurements, repeated runs gave precise results, which also matched the relevant FSI values (Figure 13).

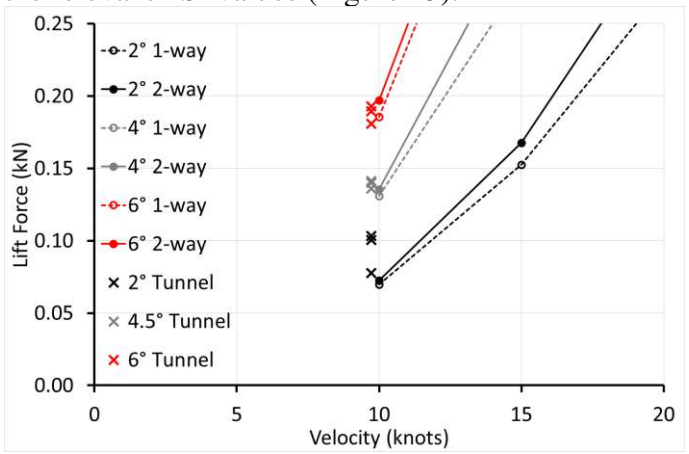


*Figure 13 Cavitation tunnel vs FSI lift force results*

The discrepancy at the lowest AoA is thought to be due to small errors in the alignment of the fin, which become more significant as AoA is reduced; during production, the fin is positioned in the base after lamination by hand and it is very possible that small errors in this mounting are present. Further tunnel testing with a digital data acquisition system will use both positive and negative angles of attack in order to identify better the zero AoA position.

Figure 14 shows a constant lift coefficient, $C_L$ (equation (3)) with velocity for the 1-way analysis as expected.

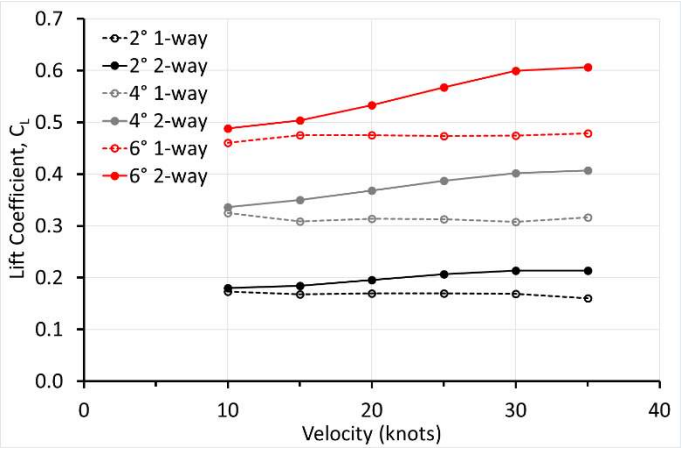


*Figure 14 Lift coefficient vs velocity*

$$C_L = \frac{2L}{\rho V^2 A} \quad (3)$$

where $L$ is lift force, $\rho$ fluid density, $V$ the flow speed and $A$ the surface area of the fin.

However, for the 2-way FSI, as velocity increases the fin deforms due to the flow in such a way that the lift coefficient is increased and increases further with velocity. Further, the 'lift slope' (the rate of change of $C_L$ with AoA, $C_L/\alpha$) follows the Prandtl equation (equation (4)) for the 1-way analysis, but the 2-way FSI again shows that as velocity increases the fin deforms due to the flow in such a way that this lift slope is increased (Figure 15).

$$\frac{C_L}{\alpha} = \frac{2\pi}{1+\frac{2}{AR}} \quad (4)$$

where: α is in radians and AR is aspect ratio (Span$^2$ / Surface Area = $37^2$ / 300 = 4.56)

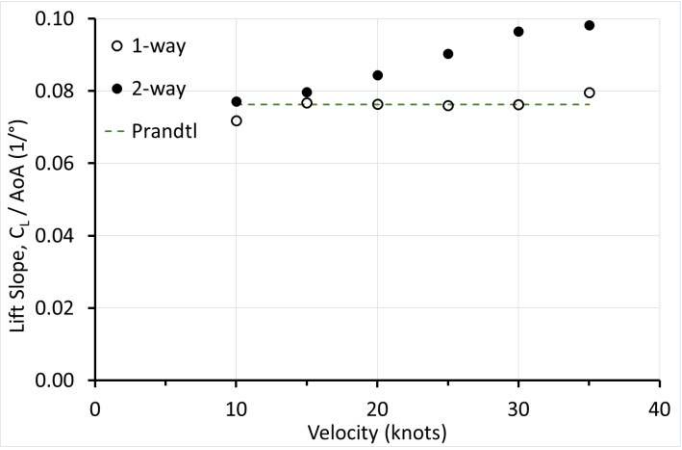


*Figure 15 Lift slope vs velocity*

Hence, for accurate prediction of the lateral 'lift', a full 2-way FSI is required, especially at higher velocities when fin deflections are large.

Drag force also increased with both velocity and AoA (Figure 8), as expected, but drag coefficient tended to decrease with velocity (Figure 16), which may be due to a reduction in skin friction drag (dominant for these streamlined chord sections) with increasing Reynold's number (Abbott and Von Doenhoff, 1959).

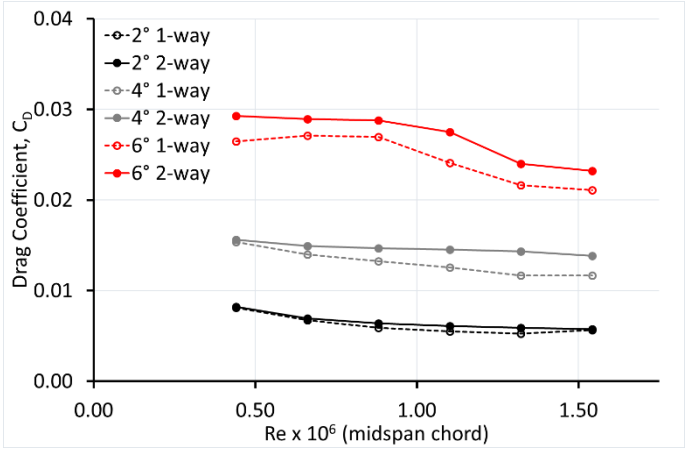


*Figure 16 Drag coefficient vs Reynolds number*

Also, the pronounced drop in drag coefficient for 6° AoA at a Reynold's number of around 1 million is typical of a reduction in the form drag component (which would be more significant at this higher AoA) as flow becomes more turbulent and hence boundary layer separation is hence delayed (Munson et al., 2009).

At lower AoA, the cheaper 1-way analysis matches the accuracy of the more expensive 2-way FSI, but at higher AoA and velocities 1-way slightly underestimates the drag estimate. Whether or not this is significant depends on the design approach, for example for comparative studies between two fin designs the 1-way analysis may be sufficient even at higher AoA.

As expected, Figure 9 shows higher lateral tip bending deflections as both AoA and velocity increases, due to the higher lateral 'lift' forces generated by the fin. The 2-way FSI deflections are slightly higher than the corresponding 1-way values, which is again consistent with the slightly higher lateral 'lift' forces predicted by the 2-way FSI.

Figure 10 shows that to predict accurately, even quantitatively, the tip twist, however, the 2-way FSI is definitely required. The one-way analysis predicts monotonically increasing wash in (increasing local AoA) as velocity (and hence tip lateral deflection) increases. However, with increasing velocity the 2-way FSI predicts an initial increase in wash-in until a maximum value at around 25 knots, followed by feathering of the foil even as far as reaching overall wash-out at higher velocities and lower AoA.

The reasons behind these effects are not yet fully understood, but they point to the possibility that there are two competing main mechanisms; bend-twist coupling due to the composite layup resulting in wash-in at higher deflections, and modification of the flow due to fin deformations that produce a wash-out axial torsional moment. The 1-way analysis (which assumes an un-deformed fin) can only include the former of these two mechanisms, leading to the deduction that the composite bend-twist coupling produces wash-in.

The 2-way FSI is also clearly necessary in accurately predicting the contribution to vertical force (as opposed to lateral 'lift' – which terminology comes from the aeronautical origins of foil theory) of the fin (Figure 11). Since the 1-way analysis does not include fin deflections it cannot predict the upwards vertical component of the fin lateral 'lift' force as the fin rotates and its suction face becomes more parallel to the water surface from its original purely vertical orientation, and in fact only predicts a small sinking force. However, the 2-way FSI predicts an increasingly significant vertical force component from the fin as velocity and AoA, and hence lateral deflections, increase (Figure 17).

*Figure 17 FSI lateral deflection for 35 knos at 4° AoA*

This is consistent with the experience of sailors sailing with too large a fin for the conditions – at speed the board becomes uncontrollably airborne resulting in the inevitable spectacularly wet (yet somehow enjoyable) crash.

## 5 CONCLUSIONS

Numerical models of a windsurf fin were developed and validated using both mechanical and water tunnel tests. Two models were made – a 'one-way' analysis (where the effects of fin deformation on the fluid flow are not considered) and a full 'two-way' FSI model (which iteratively takes into account the effect of the fin deformation on the fluid flow). A parametric study then used these models to investigate the fin behavior and performance for a wide range of typical sailing velocities and angles of attack (leeway-angles).

The more expensive two-way model was required for predicting accurately the lateral 'lift' and vertical forces, and tip twist, but reasonable predictions of the drag force (especially at lower leeway angles) and tip deflection may perhaps be obtained using the more economical one-way model.

The 2-way FSI predicts an increasingly significant vertical upwards force component from the fin as velocity and AoA increase. Two competing twist mechanisms; composite material bend-twist coupling giving wash-in (higher AoA) at higher lateral deflections, and flow modifications due to fin deformations that giving wash-out (feathering) are thought to be active.

## REFERENCES


ABAQUS, 2018. Abaqus Unified FEA-3DEXPERIENCE R2018. Dassault Systèmes, Rhode Island.

Abbott, I.H., Von Doenhoff, A.E., 1959. Theory of wing sections, including a summary of airfoil data. McGraw-Hill, New York.

Abdelal, N., Donaldson, S.L., 2018. Comparison of methods for the characterization of voids in glass fiber composites. Journal of Composite Materials 52, 487–501.

Altmann, A., 2015. Strength prediction of ply waviness in composite materials considering matrix dominated effects. Composite Structures 9.

ANSYS© 2020 R1, 2020. ANSYS Inc, Cannonsburg, PA, USA.

Broers, C., Chiu, T.W., Pourzanjani, M.M.A., Buckingham, D.J., 1992. Effects of Fin Geometry and Surface Finish on Sailboard Performance and Manoeuvrability, in: Wilson, P.A. (Ed.), Manoeuvering and Control of Marine Craft, MCMC 92. 2nd International conference, Manoeuvring and control of marine craft, Computational Mechanics Publications, Southampton, UK, pp. 275–289.

Chamis, C.C., 1984. Mechanics of composite materials past, present, and future.pdf. 21st Annual Meeting of the Society for Engineering Science, NASA, Blacksburg, Virginia, p. 41.

Chamis, C.C., 1983. Simplified composite micromechanics equations for hygral, thermal and mechanical properties. 38th Annual Conference of the Society of the Plastics Industry (SPI), NASA, Reinforced Plastics/Composites Institute, Houston, Texas, p. 19.

Chiu, T.W., Broers, C., Walker, A., Baller, C., 1993. An experimental study of the effects of deformable tip on the performance of fins and finite wings, in: 23rd Fluid Dynamics, Plasmadynamics, and Lasers Conference, Fluid Dynamics and Co-Located Conferences. American Institute of Aeronautics and Astronautics.

Chiu, T.W., Van den Bersselaar, T., Broers, C., Buckingham, D.J., 1992. The Effects of Tip Flexibility on the Performance of a Blade-Type Windsurfer Fin, in: Manoeuvering and Control of Marine Craft, MCMC 92. Presented at the 2nd International conference, Manoeuvring and control of marine craft, Computational Mechanics Publications, Southampton, UK, pp. 261–274.

Fagg, S., 1997. The development of a reversible and finitely variable camber windsurf fin (PhD). Bournemouth University, Bournemouth.

Fagg, S., Velay, X., 1996a. Simulating the operation of a novel variable camber hydrofoil, in: 1996 IEEE Aerospace Applications Conference. Proceedings. pp. 261–271 vol.3.

Fagg, S., Velay, X., 1996b. The development of a novel composite material hydrofoil through advanced computational techniques. WIT Transactions on Engineering Sciences 10.

Kunoth, A., Schlichtenmayer, M., Schneider, C., 2007. Speed windsurfing: Modeling and numerics. International Journal of Numerical Analysis and Modeling 4, 548–558.

Munson, B.R., Okiishi, T.H., Huebsch, W.W., 2009. Fundamentals of fluid mechanics, 6th ed. ed. J. Wiley & Sons, Hoboken, NJ.
Nascimento, F., Sutherland, L.S., Garbatov, Y., 2018. Experimental and numerical structural analysis of a windsurf fin, in: Guedes Soares, C., Santos, T.A. (Eds.), Progress in Maritime Technology and Engineering: Proceedings of the 4th International Conference on Maritime Technology and Engineering (MARTECH 2018), May 7-9, 2018, Lisbon, Portugal. Taylor & Francis Group, London, UK, pp. 387–394.
Nayar, K.G., Sharqawy, M.H., Banchik, L.D., 2016. Thermophysical properties of seawater: A review and new correlations that include pressure dependence 24.
Roopa, T.S., Murthy, H.N., Sudarshan, K., Nandagopan, O.R., Kumar, A., Krishna, M., Angadi, G., 2015. Mechanical properties of vinylester/glass and polyester/glass composites fabricated by resin transfer molding and hand lay-up. J Vinyl Addit Technol 21, 166–173.
Saldanha, A.R.Q., 2019. Hydrodynamic and Fluid-Structure Interaction analysis of a Windsurf Fin (MSc). Instituto Superior Técnico, Lisbon, Portugal.
Shenoi, R.A., Wellicome, J.F., West European Graduate Education Marine Technology (Eds.), 1993. Composite Materials in Maritime Structures, Volume 1 Fundamental Aspects, Cambridge ocean technology series. Cambridge University Press, Cambridge ; New York.
Siemens Simcenter STAR-CCM+ Documentation, 2019. . Siemens, Munich, Germany.
Sleight, S., 1985. Modern Boat Building Materials. Conway Maritime Press Ltd, London, UK.
Smith, C.S., 1990. Design of Marine Structures in Composite Materials. Elsevier Ltd, Barking, UK.
Sutherland, L.S., 1993. Windsurfer Fin Hydrodynamics (MSc Thesis) (MSc). University of Southampton, Southampton.
Sutherland, L.S., Wilson, P.A., 1994. Windsurfer Fin Hydrodynamics, in: Marine, Offshore and Ice Technology. Computational Mechanics Publications, pp. 51–58.
Tansley, K., 2018. Investigation into Windsurf Fin Hydrodynamics – A Practical Study (Dissertation). Newcastle University, Newcastle, UK.
Vignoli, L.L., Savi, M.A., Pacheco, P.M.C.L., Kalamkarov, A.L., 2019. Comparative analysis of micromechanical models for the elastic composite laminae. Composites Part B: Engineering 174, 106961.
World Sailing Speed Record Council, 2021. 500 Metre Records [WWW Document]. URL https://www.sailspeedrecords.com/500-metre (accessed 4.12.21).